PHOTOSPHERIC VARIABILITY OF THE LATE B-SUPERGIANT HD199478

N. Z. Ismailov, Sh. K. Ismailova*

Shamakhy Astrophysical Observatory named after N.Tusi,
Azerbaijan National Academy of Sciences, Shamakhy region, Azerbaijan

The results of spectral studies of photospheric lines of the late B-supergiant HD 199478 (B8Iae) in the visual range are presented. It was first-ever shown that the radial velocities of photospheric lines, as well as the emission component of the Hα line, to demonstrate synchronous variations. The equivalent widths variations of the photospheric lines and the emission component of the Hα line tend to be anticorrelation. The parameters of the spectral lines vary quasi-periodically which are characterized by extrema (maxima and minima). The time scales between the nearby extrema are about 25 days, and the full cycle of the quasi-period is about 45 $\pm$ 10 days. It was first-ever revealed that the photospheric lines show blue shifts relative to the mass center of the system during the HVA (High Velocity Absorption) event.The distribution of the velocity gradient along the line shows the existence mainly radial, and to a lesser level, non-radial pulsations.The D NaI line profiles often exhibit signs of accretion of matter onto the star. It was shown that the observed photometric variability of the star can also be explained by radial pulsations.

Keywords: late B – supergiants – stars, spectral variability – stars, absorption spectrum – stars, stellar wind – stars, individual – HD 199478.

1. INTRODUCTION

In order to study the possible relationship between the stellar winds and the photospheres of BA supergiants (SGs), a systematic study of the variations in the spectral parameters and profiles (line profile variation – lpv) of the absorption lines and lines that are indicators of stellar wind is necessary. The variability in photospheres and stellar winds of a group of BA supergiants was studied in detail by Kaufer et al. [9–11]. Certain shifts in the profiles of photospheric lines were found in the dynamic spectrum. The authors showed that the time scale of these

* E-mail: ismailovnshao@gmail.com

deviations is inconsistent with the periods of rotation of the stars.

One of the unusual features in the spectra of late B supergiants is the sudden appearance and disappearance of deep, blue-shifted high-velocity absorption component forming in the blue wing of the Hα line (Kaufer et al. [9,10]). The essence of this event is that suddenly a strong outflow of matter forms at the base of the stellar wind, which subsequently spreads throughout the wind. A sudden variation in the wind structure is also possible when the substance from a completely ionized state goes into a recombination state for some unknown reason. Since the shell rotates along the line of sight, all the resulting modulations (density, temperature) in the wind structure can be observed (Kaufer et al., [10]). Despite the certain progress made in these studies, it is not yet completely clear how such variations in the structure of the wind may be related with the variability at the level of the stellar photosphere.

HD199478 (HR 8020, B8Iae, V $\approx$ 5.69 mag) is the central star of the reflection nebula IC 5076. The star differs from the other B SGs in that it has an inverse distribution of radial velocities in the Balmer progression – higher members of the series have less displacements than lower members [2] – and, similar to Be stars, a double-peak Hα emission [13, 22]. According to Markova et al. [15], photospheric lines showed systematic shifts relative to the velocity of the center of the star with a characteristic time of about 20 days. In addition, these authors found a significant variation in the Hα emission and, according to 2000 data, a wide absorption was observed during 60 days, indicating to accretion and outflow of the substance. The HVA event in HD199478, simultaneously observed in the Hα and Hβ lines, was also found in [6]. Only in one season of observations, that of 2011, [6] detected high-velocity absorption with a maximum displacement of -510 kms^{-1} and a duration of at least about 13 days. These authors showed that the characteristic time of variability of the hydrogen emission lines is 22 $\pm$ 2 kms^{-1}, which is in good agreement with the data of Markova et al. [15].

The photometric behaviour of the star HD199478 is characterized by a prolonged irregular/multiperiodic variability with an amplitude of 0.15 mag in the B and V bands, over a period from 20 to 50 days [20]. The reason for such variations is not yet entirely clear.

The aim of this work, based on long-term spectral material, is to study the variability of different absorption spectral lines in the spectrum of HD 199478 and its relation, if any, with the stellar wind.

2. OBSERVATIONS

Spectral observations of the star HD 199478 were made on the 2 m telescope of the Shamakhy Astrophysical Observatory of Azerbaijan National Academy of

Sciences in 2011, 2013, 2014 and 2015. Observations were performed using an Echelle spectrometer built on the base of the Universal Astronomic Grid Spectrograph (UAGS) [17] and a CCD camera with 530×580 pixels. The optimal range of the spectrum covers the area λ4700-6700 Å. The spectral resolution is R = 14000. For an average exposure time of 900 sec, the signal to noise ratio S/N reached 200-300 near the Hα line. In the Hβ region, the S/N ratio is approximately half of this value. A description of the observing facilities, observational conditions and data processing may be found in more detail in Mikailov et al. [17] and Ismailov et al. [5, 7].

The data were processed using the DECH20T software developed at the SAO RAS [4] . Two spectra of the program star, as well as of the standards, were observed in sequence one after the other each night to be averaged. Intensity measurement uncertainties were dependent on the S/N level, being 0.5–0.7% in the Hα line region and reaching up to 1% in the Hβ line region. After processing the spectrograms, the spectral orders containing the lines to measure were cleared of the Earth's atmospheric lines.

The basic information on the obtained spectral material is summarized in Table 1. The Table provides the dates of observations, the number of spectrograms per season (year), the average S/N value for the observing run, and the average signal accumulation time.

Table 1. Brief information about the spectral material.

Observation dates	**JD 2450000+**	**Days in the run**	**N**	**S/N**	t_{exp} **(sec)**
2011 July 2–October 6	5745.40 - 5841.26	96	17	180	1100
2013 July 22–November 25	6496.28 - 6622.19	126	14	195	900
2014 June 19–September 15	6828.18 - 6916.18	90	23	200	900
2015 May 27–July 9	7173.16 – 7213.27	40	10	220	900

The results of studying the Hα and Hβ hydrogen lines for individual years based on this spectral material are presented in [6]. In this paper, we present the results of studies of the absorption photosphere lines.

In order to investigate the possible connection between the stellar wind and variations in the photosphere, it is extremely important to study wind lines (Hα), photosphere - wind transition lines (i.e., the strongest absorption lines of CII, SiII, and HeI) and to make a detailed analysis of purely photospheric lines as well. For this purpose, we measured the strongest absorption lines, such as CII λ 6578, 6583 Å, SiII λ6347, 6371 Å, HeI λ 5876, 4922 Å, D1, D2 NaI. The set of lines also includes more than 40 absorption lines related to various elements such as HeI, SiII, FeII, FeI, SII, AlIII, NaII, YII, etc.

Unlike hydrogen lines, absorption lines do not contain emission components and the profiles of these lines are almost Gaussian curves. To evaluate the intensity, the equivalent widths (EWs) of the absorption lines were measured using the method of integration.

We conventionally grouped the lines according to their EW values: the weakest lines are included in the first group with EW ≤ 0.25 Å. The second group includes lines with EW ≥ 0.25 Å. To estimate the measurement errors in EW, used the spectra of standard stars, which were obtained under the same conditions. Metal lines with equivalent widths in the range from 0.01 to 1.50 Å were selected from the spectrum of the standards. According to the spectrograms obtained for 14 nights of observations, the root-mean-square deviation of the equivalent widths varies from 10% to 2.5%, respectively. These measurements indicated that the mean uncertainty in measuring EWs of absorption lines of the star varied between 3.5–4.0%.

To measure radial velocities (RVs), we have used the cross-correlation method in which a selected section of the profile is smoothed by a cubic spline and the profile is subsequently superimposed on its mirror image produced by the program after smoothing. To get the profiles matched as good as possible, the method of shifting them respective to each other was used and the quality of the superposition obtained was controlled by the correlation coefficient. Since the wings of absorption lines were not overlapped so well as the central parts of the lines, the preference in combining mirror profiles was given to the center of the line and its lower part along the line peak. In addition, this approach allowed us to eliminate possible errors that might occur in determining the continuum level. This kind of measurements yields terms error for different lines varying between $\pm$ 1.5–2 km/s^{-1}. The reference measurements of radial velocities performed for different standard stars showed a high degree of coincidence of their measured RV values with the catalog data within ± 3 km/s^{-1}. We have not detected any systematic differences in our RV measurements for standard stars within the measure uncertainties [5].

3. MAIN RESULTS

3.1. General Variability of the Photospheric Lines

The Table 2 presents the mean parameters for each year of observations - radial velocities RV and equivalent widths EW for all measured absorption lines. For each parameter, the standard deviation is given from the mean value σ_{rms}, which is an indicator of the magnitude of the parameter variation. As can be seen from Table 1, the radial velocities of different photospheric lines show an

interval of variations from -25 to -8 kms^{-1}. If we take into account the mass center velocity of the system, which is equal to -15 km/s^{-1} [12], then the range of RV variations in the absorption lines relative to the mass center of the system will be from -10 up to +7 km/s^{-1}, respectively.

Our data showed that, this value most likely refers to the mean cluster velocity for IC 5076. Indeed, as can be seen from Table 2, the radial velocities of the weakest photospheric lines have values of -24±2 km/s^{-1} on average. We could take this value for the speed of motion of the mass center of the system, but we do not know if there is a stellar wind at this level of the photosphere, where the weakest lines are formed. In any case, this will not change the main results of this work.

We have investigated weak photospheric lines that form in the lower photosphere, being hence less influenced by wind. In addition we have considered strong photospheric lines that form in the photosphere, but can be more strongly influenced by the stellar wind, as well as the emission component of the Hα line, which is completely forms in the upper parts of the wind. As was shown in Markova &Valchev (2000) and Ismailov&Ismayilova (2019), the Hα line mostly is observed in double peak emission, with a variable relation of the V/R components.

One of the longest series of observations was made in 2014, in which 23 nights of observations were performed within 90 days (Table 1). In this section, we will consider the variability of the parameters of individual photospheric lines obtained in 2014. To detect a possible relationship in the variations in photospheric lines and lines that form in the stellar wind, we will also compare the results obtained for variations in photospheric lines with the data of the Hα line.

Figure 1 shows diagrams of variations in time for the parameters RV and EW revealed in strong absorption lines with EW≥0.25 Å according to the data through a season 2014. The bottom two panels show the parameters of the emission component of the Hα line (Fig. 6 [6]). The two lower panels from left to right show the variations in the same parameters of the absorption lines, which can also be partially under influence of the stellar wind. As can be seen from Fig. 1, the radial velocities of strong absorption lines are vary smoothly and synchronously with the Hα line emission. The minimum in the RV curve for the Hα line is reached on JD 2456843, and the maximum on JD 24566869, the interval between them is approximately 26 days. The minimum on the RV curve along the indicated absorption lines occurs on JD 24566860, and the maximum is around JD 24566877, that is, in about 27 days.

Figure 1 demonstrates that the variation in the EW parameter for the Hα emission is synchronous with its radial velocity, and the dates of their maximum and minimum coincide. The absorption lines show different patterns of EW variations relative to the Hα line. For example, in the region of the maximum EW

Table 2. Seasonally averaged parameters of some photospheric spectral lines of the star HD 199478

Elements	λ (Å)	2011				2013			
		RV (km/s^{-1})	σ (km/s^{-1})	EW (Å)	σ (Å)	RV (km/s^{-1})	σ (km/s^{-1})	EW (Å)	σ (Å)
NaI	5889.95	-15.9	2.3	0.90	0.34	-14.6	2.2	0.87	0.012
Na I	5895.92	-15.8	2.1	1.19	0.18	-12.4	2.0	0.73	0.025
Na II	5688.21	-14.5	1.9	0.15	0.010	-16.1	4.6	0.15	0.010
C II	6578.05	-20.3	1.4	0.31	0.06	-17.9	4.3	0.24	0.017
C II	6582.88	-21.0	1.5	0.32	0.03	-16.8	4.2	0.22	0.019
HeI	4921.93	-18.5	2.7	0.45	0.042	-14.8	3.1	0.40	0.019
HeI	5015.68	-25.8	2.1	0.22	0.011	-14.8	1.6	0.23	0.039
HeI	5047.71	-21.1	2.8	0.15	0.007	-15.2	2.7	0.15	0.010
HeI	5875.62	-17.2	2.7	0.98	0.105	-12.4	1.4	0.74	0.013
Fe II	5018.44	-19.8	1.8	0.05	0.002	-17.9	1.8	0.02	0.017
Fe II	5276.001	-21.9	1.8	0.05	0.001	-20.9	2.0	0.03	0.001
Fe II	5316.23	-19.3	0.7	0.13	0.009	-18.3	0.8	0.14	0.010
Fe II	5482.31	-20.4	2.8	0.02	0.003	-19.2	2.7	0.05	0.002
Fe II	5487.62	-19.9	2.7	0.02	0.004	-19.6	2.5	0.02	0.003
Si II	5041.02	-23.5	1.3	0.21	0.025	-19.8	1.1	0.22	0.023
Si II	5055.98	-25.9	3.9	0.23	0.019	-22.4	2.4	0.25	0.010
Si II	6347.11	-23.1	2.4	0.85	0.071	-22.8	2.5	0.66	0.021
Si II	6371.37	-23.3	2.5	0.79	0.063	-23.1	2.7	0.53	0.017
S II	5212.62	-22.0	1.7	0.07	0.003	-20.2	1.5	0.05	0.002
S II	5320.73	-21.5	2.0	0.05	0.005	-19.6	2.2	0.06	0.002
S II	5453.86	-21.3	2.7	0.22	0.02	-20.0	2.9	0.20	0.038
S II	5009.57	-21.1	1.6	0.22	0.009	-20.0	1.2	0.22	0.016
S II	5032.43	-25.0	1.0	0.14	0.008	-20.7	0.4	0.15	0.012
S II	5432.8	-24.9	1.5	0.15	0.007	-22.3	1.4	0.15	0.007
S II	5639.97	-19.4	0.8	0.19	0.013	-20.1	1.5	0.18	0.008
S II	5647.03	-23.5	1.0	0.13	0.009	-19.2	1.1	0.13	0.008
S II	5212.62	-24.5	1.6	0.07	0.005	-20.7	1.7	0.05	0.005
S II	5320.73	-23.8	1.8	0.06	0.005	-21.8	1.5	0.07	0.003
S II	5345.72	-24.2	1.7	0.08	0.001	-20.8	1.8	0.08	0.002
S II	5428.67	-25.0	1.3	0.07	0.004	-22.5	1.3	0.06	0.004
S II	5606.15	-24.3	1.2	0.08	0.004	-20.9	1.3	0.09	0.004
S II	5659.99	-24.3	1.7	0.05	0.005	-16.8	2.9	0.06	0.005
S II	5664.78	-23.3	1.1	0.05	0.004	-19.1	2.6	0.07	0.005
Al III	5696.61	-21.3	1.7	0.14	0.021	-9.8	2.6	0.15	0.011
Y II	5473.38	-16.0	1.3	0.08	0.002	-18.9	2.3	0.09	0.024
Y II	5509.9	-24.1	4.0	0.13	0.012	-21.7	2.9	0.14	0.015
Fe I	5168.9	-23.8	3.3	0.23	0.012	-19.2	2.5	0.23	0.011
Fe I	5127.36	-23.4	3.6	0.09	0.011	-22.0	2.8	0.08	0.037
Fe III	5156.12	-23.2	3.6	0.06	0.007	-19.9	2.2	0.06	0.005
DIB	5780.63	-23.7	2.1	0.43	0.013	-16.0	2.8	0.42	0.013
DIB	5796.96	-15.8	3.0	0.12	0.010	-8.1	4.9	0.14	0.011
Cr I	5206.04	-19.2	1.6	0.01	0.018	-18.4	1.3	0.01	0.002
Cr II	5279.95	-19.6	1.7	0.02	0.002	-23.2	1.6	0.02	0.001

	2014					2015			
Na I	5889.95	-15.6	1.4	0.84	0.033	-13.3	7.3	0.82	0.01
NaI	5895.92	-14.5	1.6	0.72	0.034	-12.0	6.3	0.70	0.02
Na II	5688.21	-14.8	1.5	0.17	0.023	-18.1	5.5	0.14	0.010
C II	6578.05	-19.9	3.4	0.25	0.017	-21.7	4.1	0.23	0.01
C II	6582.88	-19.8	3.9	0.22	0.015	-21.9	5.2	0.21	0.01
HeI	4921.93	-19.9	2.9	0.47	0.031	-19.0	8.9	0.43	0.009
HeI	5015.68	-23.5	1.3	0.26	0.012	-23.7	2.4	0.25	0.007
HeI	5047.71	-21.5	2.6	0.18	0.018	-21.7	1.0	0.16	0.005
HeI	5875.62	-11.1	4.6	0.72	0.022	-11.5	6.5	0.78	0.021
Fe II	5018.44	-22.0	1.6	0.04	0.004	-19.6	15.1	0.06	0.002
Fe II	5276.001	-22.3	1.6	0.06	0.002	-24.7	1.2	0.04	0.002
Fe II	5316.23	-20.3	1.3	0.15	0.002	-21.9	0.6	0.14	0.010
Fe II	5482.31	-21.8	1.8	0.05	0.010	-22.9	1.8	0.04	7.326
Fe II	5487.62	-21.8	1.7	0.02	0.003	-22.5	2.2	0.03	0.003
Si II	5041.02	-25.5	1.7	0.24	0.017	-23.7	2.2	0.23	0.024
Si II	5055.98	-25.2	2.1	0.27	0.014	-23.6	1.9	0.25	0.014
Si II	6347.11	-20.5	3.6	0.68	0.018	-21.3	3.6	0.69	0.007
Si II	6371.37	-20.4	3.7	0.55	0.010	-22.5	3.3	0.51	0.027
S II	5212.62	-22.2	1.4	0.05	0.003	-25.2	3.1	0.06	0.004
S II	5320.73	-21.8	2.0	0.05	0.004	-20.1	2.0	0.04	0.002
S II	5453.86	-21.5	2.1	0.21	0.021	-24.1	1.4	0.21	0.021
S II	5009.57	-22.5	1.8	0.24	0.030	-25.8	3.6	0.21	0.020
S II	5032.43	-24.1	1.1	0.15	0.015	-26.5	4.1	0.16	0.015
S II	5432.8	-24.3	1.2	0.18	0.018	-24.5	1.5	0.19	0.017
S II	5639.97	-20.1	1.9	0.19	0.015	-21.2	0.9	0.21	0.024
S II	5647.03	-22.8	2.1	0.14	0.013	-22.9	0.8	0.15	0.012
S II	5212.62	-24.7	1.0	0.05	0.004	-25.5	1.6	0.06	0.005
S II	5320.73	-24.3	1.3	0.06	0.004	-24.8	1.3	0.07	0.001
S II	5345.72	-24.3	1.4	0.08	0.002	-25.0	1.1	0.08	0.002
S II	5428.67	-24.9	1.3	0.07	0.003	-24.0	1.4	0.08	0.003
S II	5606.15	-24.0	1.3	0.09	0.004	-23.0	1.0	0.08	0.002
S II	5659.99	-23.0	2.9	0.05	0.005	-20.0	2.5	0.06	0.003
S II	5664.78	-21.9	2.7	0.06	0.007	-	-	-	-
Al III	5696.61	-21.3	1.4	0.15	0.027	-18.9	5.0	0.18	0.018
YII	5473.38	-24.7	2.9	0.11	0.014	-21.5	2.5	0.12	0.002
YII	5509.9	-24.7	2.9	0.15	0.014	-22.1	2.2	0.08	0.019
FeI	5168.9	-26.5	3.4	0.24	0.018	-23.8	2.0	0.24	0.007
FeI	5127.36	-24.8	2.6	0.07	0.009	-23.4	2.1	0.10	0.011
Fe III	5156.12	-24.8	2.0	0.05	0.007	-23.4	1.7	0.07	0.005
DIB	5780.63	-23.2	1.9	0.43	0.014	-15.3	5.3	0.41	0.007
DIB	5796.96	-15.5	2.1	0.14	0.008	-7.9	7.8	0.12	0.019
Cr I	5206.04	-24.5	1.5	0.01	0.002	-21.9	1.5	0.02	0.007
CrII	5279.95	-24.0	2.1	0.02	0.002	-24.1	1.7	0.03	0.002

Table 3. Time variation parameters of 2011 data.

Atom	λ (Å)	Max, JD 2455000	RV, (kms^{-1})	Min, JD 2455000	RV (kms^{-1})	Max, JD 2455000	EW, (Å)	Min, JD 2455000	EW (Å)	Δt (RV) days	Δt (EW) days
HeI	4921	768	-15	808	-23	768	0.5	788	0.47	40	20
HeI	5015	762	-23	808	-29	749	0.2	788	0.23	46	39
HeI	5047	764	-17	809	-26	747	0.14	771	0.16	45	24
HeI	5876	762	-12	808	-20	747	0.88	757	1.06	46	10
Fe II	5018	745	-17	762	-23	749	0.05	789	0.056	17	40
Fe II	5276	745	-18	771	-24	762	0.02	776	0.018	26	14
Fe II	5316	745	-18	768	-20	745	0.12	769	0.15	23	24
Fe II	5482	745	-16	788	-25	745	0.015	789	0.023	43	44
Fe II	5487	745	-16	768	-24	756	0.019	808	0.03	23	52
Si II	5041	747	-22	788	-32	745	0.04	762	0.05	41	17
Si II	5056	749	-26	769	-25	745	0.038	771	0.052	20	26
S II	5010	750	-18	768	-22	757	0.21	789	0.18	18	32
S II	5032	747	-23	776	-26	747	0.13	776	0.15	29	29
S II	5640	750	-18	776	-20	749	0.2	768	0.18	26	19
S II	5647	747	-22	762	-25	756	0.14	768	0.12	15	12
S II	5433	745	-22	769	-26	749	0.14	768	0.16	24	19
S II	5454	745	-18	769	-23	747	0.19	769	0.16	24	22
S II	5606	747	-23	762	-26	745	0.099	769	0.085	15	24
S II	5660	745	-18	762	-25	747	0.044	769	0.057	17	22
S II	5665	745	-20	762	-24	757	0.056	789	0.049	17	32
S II	5213	745	-20	771	-26	764	0.049	808	0.059	26	44
S II	5321	747	-22	771	-27	745	0.058	764	0.069	24	19
S II	5346	745	-21	789	-26	745	0.08	756	0.075	44	11
S II	5429	745	-22	771	-27	745	0.079	762	0.069	26	17
Na II	5688	745	-13	762	-19	747	0.16	768	0.13	17	21
Al III	5697	745	-16	764	-23	745	0.16	769	0.09	19	24
Y II	5473	745	-14	756	-18	750	0.057	776	0.069	11	26
Fe II	5169	745	-17	769	-27	749	0.2	776	0.24	24	27
Fe II	5127	747	-14	769	-26	757	0.07	788	0.12	22	31
Fe III	5156	745	-15	771	-26	757	0.047	788	0.07	26	31
Mean										26	26
σ rms										10	10

values of the Hα line, a minimum is observed for the lines HeI λ4921 Å,CII λ 6578, 6583 Å, and Si II λ 6347, 6371 Å, i.e. there is an anticorrelation tendency. The D1, D2 NaI and HeI λ 5876 Å lines exhibit a slight increase in the region where the EW maximum of the Hα line is observed, suggesting a direct correlation. This indicates that the D NaI and HeI λ 5876 Å lines are influenced by the upper part of the stellar wind. The cyclical nature of EW variations in the strongest absorption lines indicates that the stellar wind may exert an influence on these lines.

Table 4. Time variation parameters of 2014 data.

Atom	λ (Å)	Min, JD 2455000	RV, (kms^{-1})	Max, JD 2455000	RV (kms^{-1})	Min, JD 2455000	RV, (kms^{-1})	Δt_2 days	Δt_2 days	T, days
HeI	4921	830	-23	863	-15	879	-23	33	16	49
He I	5015	830	-24	877	-28	916	-24	47	39	86
HeI	5047	828	-24	862	-17	879	-25	34	17	51
HeI	5876	828	-15	862	-17	880	-20	34	18	52
Fe II	5018	836	-20	862	-24	888	-19	26	26	52
Fe II	5276	836	-21	864	-25	888	-20	28	24	52
Fe II	5316	835	-18	855	-22	880	-18	20	25	45
Fe II	5482	856	-19	875	-24	888	-20	19	13	32
Fe II	5487	842	-21	862	-25	888	-19	20	26	46
Si II	5041	843	-25	876	-27	888	-22	33	12	55
Si II	5056	843	-22	864	-28	888	-23	21	24	45
SII	5010	828	-26	856	-18	882	-25	28	26	54
SII	5032	830	-25	856	-23	876	-26	26	20	46
SII	5640	828	-17	851	-24	875	-17	23	24	47
SII	5647	828	-16	855	-24	875	-23	27	20	47
SII	5433	835	-25	850	-22	875	-26	15	25	40
SII	5454	835	-25	862	-23	876	-26	27	14	41
SII	5606	842	-24	850	-23	864	-26	14	15	29
SII	5660	828	-15	869	-25	888	-24	41	19	60
SII	5665	864	-24	830	-16	888	-23	34	58	92
SII	5213	830	-25	843	-23	862	-25	13	19	32
SII	5321	835	-25	850	-22	876	-26	15	26	41
SII	5346	835	-25	850	-21	882	-26	15	32	47
SII	5429	830	-25	850	-22	879	-27	20	29	49
SII	5688	835	-18	880	-12	864	-19	45	16	61
Na II	5697	836	-20	863	-23	888	-19	27	25	52
AlIII	5473	862	-27	888	-18	864	-23	26	24	50
YII	5169	835	-32	855	-22	875	-28	20	20	40
Fe II	5127	842	-27	855	-21	888	-26	13	20	33
Fe III	5156	842	-27	856	-22	916	-29	13	33	46
Mean								25	24	49
σ_{rms}								9	9	13
EW		Min 2455000	EW (Å)	Max 2455000	EW (Å)	Min 2455000	EW (Å)	Δt_1 days	Δt_2 days	T, days
HeI	4921	842	0.42	863	0.51	875	0.46	21	12	33
HeI	5015									
HeI	5047	842	0.16	869	0.22	908	0.16	27	39	66
HeI	5876	856	0.68	880	0.76	916	0.72	24	36	60
HeI	5018	828	0.026	850	0.019	877	0.032	22	27	49
Fe II	5276	856	0.058	875	0.055	888	0.058	19	13	32
Fe II	5316	842	0.018	855	0.02	875	0.018	13	20	33
Fe II	5482	842	0.13	862	0.15	879	0.12	20	17	37
Fe II	5487	828	0.023	856	0.018	877	0.026	28	21	49
Si II	5041	842	0.23	863	0.26	876	0.23	21	13	34

Si II	5056	842	0.25	864	0.29	877	0.25	22	13	35
SII	5010	842	0.22	862	0.28	882	0.19	20	20	40
SII	5032	851	0.13	830	0.18	875	0.13	21	45	66
SII	5640	850	0.16	856	0.2	869	0.18	14	13	29
SII	5647	843	0.13	888	0.16	869	0.12	25	13	48
SII	5433	830	0.17	843	0.21	863	0.15	13	20	33
SII	5454	828	0.2	855	0.24	879	0.17	27	24	51
SII	5606	836	0.094	828	0.14	877	0.085	26	32	58
SII	5660	851	0.044	830	0.06	888	0.048	21	58	79
SII	5665	855	0.054	830	0.07	888	0.049	25	58	83
SII	5213	850	0.048	882	0.059	875	0.049	15	13	28
SII	5321	850	0.058	869	0.069	880	0.059	19	11	30
SII	5346	830	0.079	842	0.083	862	0.075	12	20	32
SII	5429	830	0.07	850	0.079	877	0.068	20	27	47
Na II	5688	828	0.18	851	0.22	875	0.14	23	24	47
AlIII	5697	828	0.2	851	0.15	862	0.16	23	11	34
YII	5473	855	0.057	888	0.08	875	0.06	33	13	46
Fe II	5169	828	0.27	851	0.2	877	0.24	23	26	49
Fe II	5127	830	0.088	850	0.06	888	0.085	20	38	58
Fe III	5156	843	0.047	856	0.035	879	0.038	13	23	36
Mean								21	24	46
σ_{rms}								5	13	15

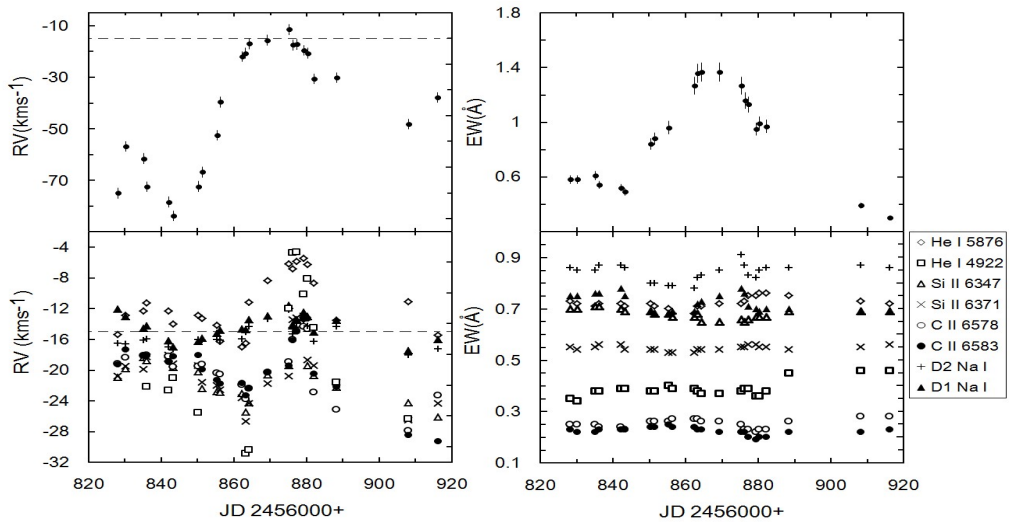

Fig. 1. Time variation of RV and EW parameters for absorption with EW $\geq$0.25 Å in 2014. The dashed horizontal lines in the left panels indicate the mass center velocity of the star.

Figure 2 shows the time variation diagrams for RV (left panels) and EW (right panels) parameters for the absorption lines FeII, SiII, and SII. As can be seen from

Table 5. Results of TVS analysis of some spectral lines.

N of lines	Lines (Å)	Vb (kms^{-1})	v_1 (kms^{-1})	Vc (kms^{-1})	v_2 (kms^{-1})	Vr (kms^{-1})	$v_2 - v_1$ (kms^{-1})	Vr-Vb (kms^{-1})	a_1	a_2	FWHM (Å)
2011											
1	C II 6578	-109	-67	-57	-26	5	41	113	0.031	0.03	2.032
2	C II 6583	-102	-72	-61	-21	10	51	112	0.024	0.029	2.016
3	Si II 6347	-98	-53	-30	-7	50	45	148	0.037	0.039	1.925
4	Si II 6371	-89	-45	-34	-11	53	34	143	0.031	0.028	1.865
5	HeI 5876	-93	-46	-31	-5	71	41	163	0.047	0.036	2.285
6	D2 Na I	-70	-24	-13	6	33	30	103	0.233	0.207	0.9
7	D1 NaI	-66	-32	-9	9	25	41	91	0.213	0.198	0.893
8	S II 5010	-	-39	-17	3	196	42	-	0.023	0.02	-
9	HeI 5016	-97	-61	-14	10	58	72	156	0.025	0.044	2.201
10	Fe II 5018	-107	-47	-12	12	95	59	202	0.029	0.025	1.593
11	Fe II 5027	-98	-56	-31	5	66	61	164	0.010	0.014	1.374
12	S II 5429	-82	-36	-13	11	69	46	151	0.016	0.016	1.465
13	S II 5433	-117	-60	-25	-2	32	57	149	0.013	0.011	1.664
14	S II 5454	-64	-42	-19	15	71	57	136	0.018	0.019	1.413
15	Y II 5474	-93	-37	-8	27	119	64	212	0.029	0.03	1.37
16	S II 5032	-97	-67	-35	11	16	78	112	0.01	0.008	1.557
17	S III 5041	-117	-60	-25	-2	32	57	149	0.013	0.011	1.538
18	He I 5048	-89	-44	-22	11	45	55	133	0.017	0.018	1.522
19	S III 5056	-56	-45	-13	8	41	54	97	0.01	0.014	1.881
	Mean	-91	-49	-25	3	57	52	141	0.044	0.042	1.639
	σ_{rms}	18	13	15	13	44	12	33	0.064	0.057	0.390
2013											
1	C II 6578	-81	-39	3	24	55	63	136	0.027	0.02	1.833
2	C II 6583	-124	-51	-18	1	22	52	145	0.028	0.021	2.275
3	Si II 6347	-114	-45	-11	24	81	69	195	0.087	0.076	1.943
4	Si II 6371	-116	-49	-16	17	84	66	199	0.067	0.061	2.118
5	HeI 5876	-130	-59	-12	23	82	83	213	0.066	0.068	2.314
6	D2 NaI	-75	-40	-17	-5	30	35	104	0.242	0.23	1.139
7	D1 NaI	-78	-32	-20	3	37	35	115	0.21	0.21	1.356
8	S II 5010	-	-	-	-	-	-	-	-	-	-
9	HeI 5016	-197	-63	-39	22	58	85	255	0.025	0.044	2.837
10	Fe II 5018	-107	-59	-23	14	134	72	240	0.024	0.033	1.812
11	Fe II 5027	-33	-41	-14	15	61	35	94	0.011	0.013	1.783
12	S II 5429	-143	-74	-30	11	-4	58	138	0.019	0.015	1.671
13	S II 5433	-152	-72	-37	-14	-3	57	149	0.028	0.027	1.661
14	S II 5454	-170	-81	-28	19	-4	67	166	0.034	0.033	1.612
15	Y II 5474	-148	-85	-32	22	2	96	150	0.014	0.014	1.368
16	S II 5032	-74	-57	-24	19	54	47	129	0.02	0.011	1.765
17	S III 5041	-75	-52	-6	52	17	103	92	0.015	0.014	1.931
18	He I 5048	-74	-40	-6	28	85	68	159	0.012	0.011	1.337
19	S III 5056	-66	-48	-12	34	68	45	134	0.018	0.022	1.698
	Mean	-109	-55	-19	17	48	63	156	0.053	0.051	1.816
	σ_{rms}	43	15	11	15	38	20	47	0.067	0.065	0.400

2014											
1	C II 6578	-74	-42	-21	10	52	52	126	0.025	0.024	1.849
2	C II 6583	-74	-42	-11	20	51	62	125	0.023	0.025	2.066
3	Si II 6347	-119	-49	-15	20	78	69	197	0.064	0.07	1.89
4	Si II 6371	-112	-45	-12	22	66	67	179	0.049	0.06	1.852
5	He I 5876	-102	-55	-20	5	74	82	176	0.077	0.084	2.297
6	D2 NaI	-77	-41	-18	4	107	34	184	0.423	0.354	1.579
7	D1 NaI	-71	-37	-14	19	77	34	148	0.393	0.332	1.566
8	S II 5010	-	-53	-22	24	100	88	-	0.018	0.022	2.227
9	HeI 5016	-109	-61	-25	-1	47	60	156	0.027	0.033	1.804
10	Fe II 5018	-118	-71	-35	1	60	71	179	0.029	0.026	1.794
11	Fe II 5027	-50	-39	-27	20	43	59	94	0.01	0.011	1.767
12	S II 5429	-91	-56	-22	1	25	58	115	0.014	0.012	1.669
13	S II 5433	-100	-54	-31	3	49	23	103	0.02	0.021	1.867
14	S II 5454	-109	-65	-31	2	35	66	144	0.038	0.04	1.611
15	Y II 5474	-100	-46	-25	4	18	32	118	0.016	0.016	1.953
16	S II 5032	-105	-59	-37	-13	11	46	116	0.013	0.017	1.75
17	S III 5041	-122	-76	-43	-19	27	46	148	0.017	0.015	1.533
18	He I 5048	-135	-90	-36	-17	1	56	135	0.018	0.015	1.707
19	S III 5056	-142	-86	-24	-15	36	56	178	0.027	0.023	1.874
	Mean	-101	-56	-25	5	50	56	146	0.068	0.063	1.824
	σ_{rms}	24	15	9	14	29	17	31	0.121	0.101	0.208
2015											
1	C II 6578	-150	-78	-26	6	48	104	198	0.018	0.022	2.053
2	C II 6583	-58	-77	-35	8	96	82	154	0.021	0.016	2.265
3	Si II 6347	-166	-74	-31	15	52	69	218	0.032	0.042	1.941
4	Si II 6371	-112	-68	-35	-2	42	66	155	0.033	0.027	1.878
5	HeI 5876	-126	-67	-20	15	74	82	200	0.059	0.059	2.532
6	D2 Na I	-99	-41	-29	-18	28	23	127	0.223	0.226	1.131
7	D1 NaI	-92	-47	-35	-12	33	34	126	0.23	0.21	0.898
8	S II 5010	-	-	-	-	-	-	-	-	-	-
9	HeI 5016	-176	-66	-48	19	67	85	243	0.047	0.052	2.201
10	Fe II 5018	-98	-61	-25	11	107	72	205	0.044	0.043	1.593
11	Fe II 5027	-82	-70	-28	24	72	94	154	0.014	0.022	1.374
12	S II 5429	-163	-79	-35	19	11	58	174	0.015	0.012	1.683
13	S II 5433	-159	-71	-26	22	26	69	185	0.022	0.022	1.674
14	S II 5454	-168	-85	-36	14	22	56	190	0.02	0.025	1.625
15	Y II 5474	-96	-82	-27	33	14	37	110	0.011	0.01	1.382
16	S II 5032	-86	-51	-27	8	54	59	140	0.026	0.029	1.557
17	S III 5041	-97	-62	-27	7	52	69	149	0.037	0.033	1.538
18	He I 5048	-72	-59	-15	19	64	78	136	0.028	0.032	1.522
19	S III 5056	-75	-52	-7	36	92	88	167	0.047	0.04	1.881
	Mean	-115	-66	-28	13	53	68	168	0.052	0.051	1.707
	σ_{rms}	38	13	9	14	28	21	36	0.065	0.062	0.404

the top left panel of Fig. 2, the radial velocities of the FeII lines mainly show a course of variations that is reverse with the radial velocities of the Hα emission, except when the maximum of the FeII λ5316 Å line is reached simultaneously with the Hα line.

The SiII lines, as the FeII lines, clearly exhibit the wavelike variation in the RV and EW parameters, the amplitude of which is much larger than the values of the measurement uncertainties. Both SiII λ5041 Å and λ5056 Å lines have a course of variations that is reverse with the Hα line, being in the same phase with the SiII λ6347 Å and λ6371 Å lines (Fig. 1).

The right panels in Fig. 2 show the time variations of the EW values of the Fe II, SiII, and SII lines. Weak absorption lines Fe II and SII show insignificant variations in EW (Fig. 3). EW variations of the SII λ5606 Å, λ5665 Åand FeII λ 5482 Ålines show minima at the moment when EW of the Hα line reaches maximum.

As can be seen from the middle panel in Fig.2 for the SiII λ5041 and 5056 Å lines, the RV parameters (left panel) and EW parameters (right panel) show reverse cyclic variations with phase - when the RV values are maximal (JD 2456243), the EW parameter reaches minimum. The time interval between two extrema is 40-45 days. On the whole, these results show that the star's variability is of quasicyclic character.

In Table 3 and Table 4, is given the information on the characteristic times of variations in the RV and EW parameters according to the data of the longest seasons - 2011 and 2014. These tables list the lines with clear cyclical variations. The 2011 observations allowed us to cover only two extrema, for example, one minimum and one maximum. The last columns present the differences between the dates of extrema δt for the RV and EW parameters. The last line of the table shows the mean value of the time interval between two extremum points. As can be seen from Table 3, for both RV and EW variations, the mean value between the two extrema is 26 $\pm$ 10 days. This timescale can be considered as half of the cycle of variations.

The 2014 season made it possible to detect three extremum dates on the cycles (min-max-min, or vice versa, max-min-max), according to the variation in the parameters of various absorption lines (see Fig. 1 and 1). Similarly to Table3, Table 4 also shows the dates of the extrema of the selected lines, as well as the differences between two adjacent extrema Δt_1 and Δt_2, and the total times T between the first and last extrema. The first part of Table 4 presents the RV data, and the bottom second part of Table 4 contains the EW parameter data. As can be seen from Table 4, the timescales between the radial velocity extrema are 25 $\pm$ 9 days and 24 $\pm$ 9 days, making up 49 days for a full cycle, and the timescales for equivalent widths are 21 $\pm$ 5 days and 24 $\pm$ 13 days, making up 46 $\pm$ 15 days

for a full cycle. The results of Tables 3 and Table 4 show that a timescale of 20-25 days may be taken for a half-cycle and a span of about 40-50 days for a full cycle. Unfortunately, we do not have data that would be covering two complete cycles. Figure 2 also demonstrates cyclical variations in the EW and RV parameters of

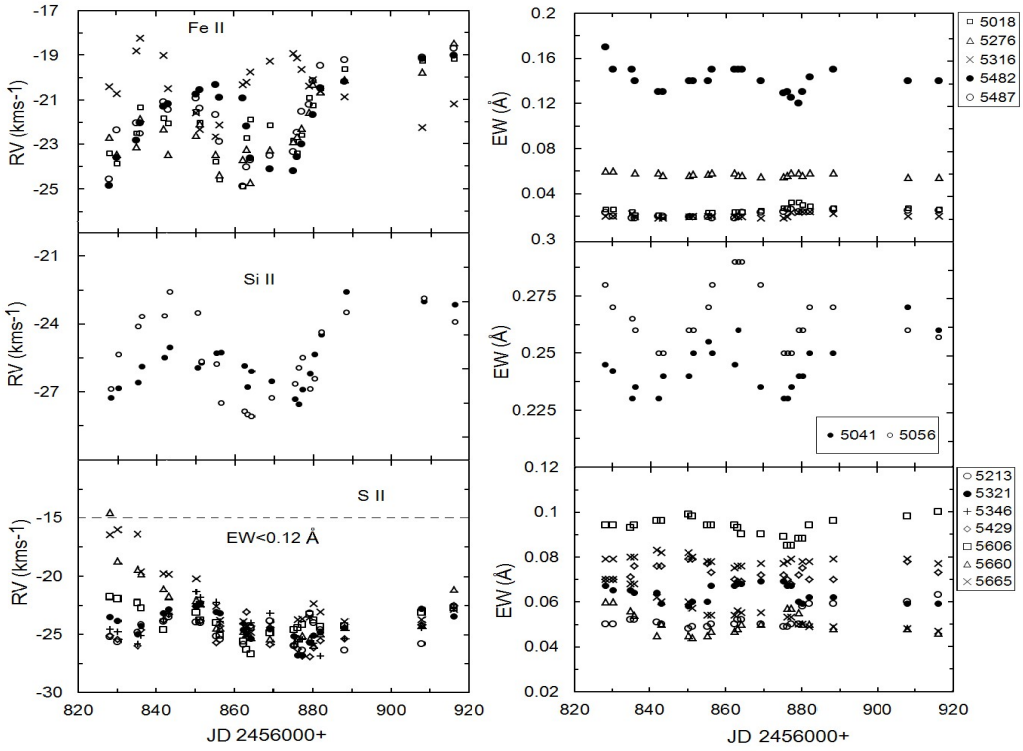

Fig. 2. Variations in time of the RV (left side) and EW (right side) parameters of absorption lines Fe II (top panels), S II (middle panels) and Si II lines (bottom panels) for the 2014 data. The dashed horizontal line in the left panel indicate the mass center velocity of the star.

the absorption lines. The characteristic time between the first and second extrema (i.e., from the minimum to the maximum, or vice versa, from the maximum to the minimum) is about 20-25 days. This characteristic time confirms the results of previous works (see, for example, Markova et al. 2008, Ismailov &Ismayilova 2019), where a 20-22 day timescale for Hα line variations was detected.

3.2. The Detection of Line-Profile Variations

It is interesting to study the line-profile variations (LPV) along the profile of the photospheric spectral lines. For this purpose we used a statistical method

that was applied by Prinja et al. (1996) and was named the temporal variance spectrum (TVS) (Fullerton et al., 1996). This method was applied to analyze the radial velocity and intensity variability along the spectral line profiles (see, for example, Kaufer et al., 1997, Markova &Valchev, 2008). The method consists of calculating the root mean square (rms) of a series of spectrograms at a given wavelength of the spectral line profile as a function of wavelength σ_λ.

Figure 3 shows the average profiles of individual strong absorption lines observed in different parts of the spectrum for the 2014 season, as well as the profile of the TVS spectrum σ_λ obtained from the data of 23 spectrograms. As can be seen, the average profiles of the D NaI lines have relatively asymmetric red wings. The other absorption lines show a symmetrical structure. Here, in the TVS plots, the vertical dashed and solid lines schematically mark the boundaries within which the indicated parameters were calculated from each profile at a given wavelength. From the mean line profile the full line width at the half level of the residual intensity FWHM was measured. From the TVS profile, the border radial velocities Vb (blue) and Vr (red) were calculated at the level of the variability threshold with a significance level p = 1% relative to the continuum, their difference is ΔV = Vr-Vb. For each TVS spectrum, the velocities $v_1 and v_2$ corresponding to each peak, the velocity of the central dip Vc between the profile peaks and the velocity difference Δv = v_2-v_1 were measured, as well as the a_1 and a_2, values corresponding to the σ_λ parameters for individual peaks. Table 3.1 shows a list of the groups with strong and weak photospheric lines, for which all the indicated parameters were obtained for all individual observation seasons.

To control the instrumental displacements, from the longest series of observations carried out over 23 nights in 2014, we plotted the average profile of the λ6520 - 6560 Å spectral region, containing weak H2O lines of the Earth's atmosphere, the intensity of which is between 3-12% of the average continuum (left top panel in Fig.3). Since these lines are stable in wavelength, the TVS structures of the atmospheric lines show single peaks, in which σ_λ variations are only due to variations in the line intensities.

As we can see from Fig. 3, all TVS profiles of the absorption lines have two peaks with a central dip. Two peaks observation in the TVS spectra of the spectral lines indicate that in the main variability interval ΔV occurs on the line wings, and to a lesser degree in other parts of the profile. The velocities corresponding to the peaks v1 and v2 in the TVS spectra show the most probable values of the RV gradient (variations) along the spectral line. If we assume the pulsating nature of the observed LPV, then the appearance of two strongest peaks and weaker sections in the TVS line profile indicates the simultaneous existence of radial and non-radial pulsations. Non-radial pulsations are the main contributors to the center of the line TVS profile. Radial modes only contribute to the line

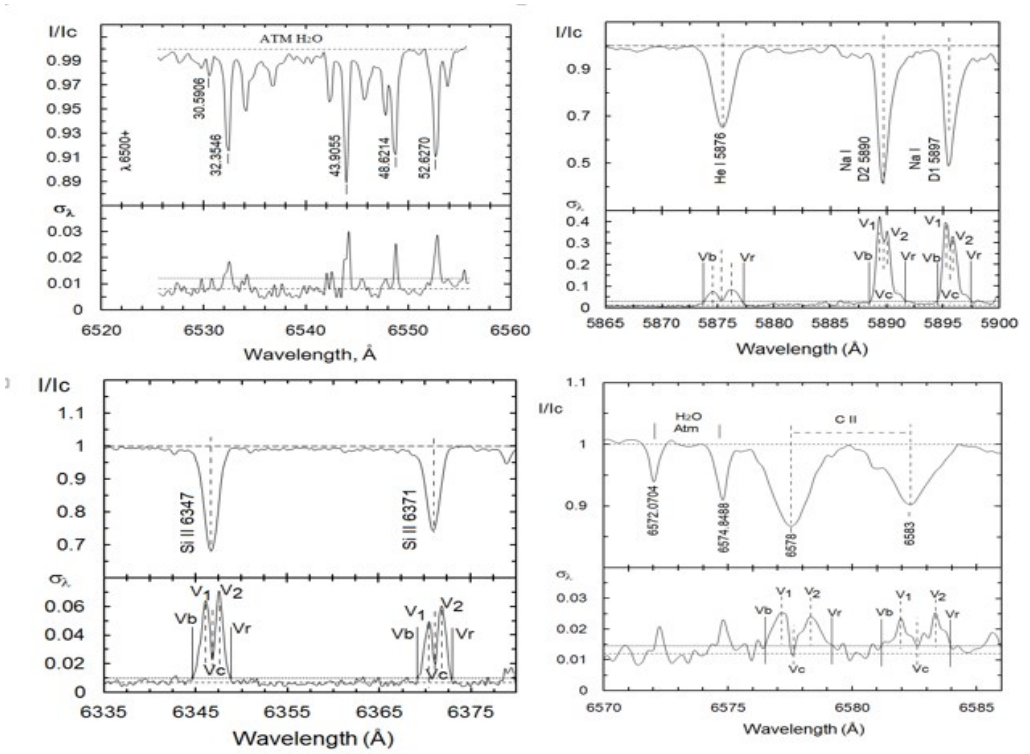

Fig. 3. Profiles of individual ranges of the star's spectrum, averaged over 23 nights of observations using the 2014 data, with the corresponding TVS spectra of these ranges. The top left diagram is plotted only for telluric lines. In each TVS spectrum, the horizontal bold dashed lines indicate the mean continuum level and the dotted lines correspond to the level of the variability threshold equal to p = 1%. On the TVS profile of each line, the wavelength boundaries used to calculate the parameters presented in Table 6 are indicated.

wings, where the gradient in the line profile is strongest (see, for example, [11]).

Figures 4 and 5 based on the 2014 data, demonstrate also average profiles of two different parts of the star's spectrum, which contain a group of weak photospheric lines. As can be seen, the TVS structure of weak lines is almost the same as that of strong lines. In Table 5, where is presented all TVS analysis parameters, the lines with EW$\geq$0.25 Å are marked in bold. The rest of the lines in the list have EW$\leq$0.25 Å,i.e.
belong to the first group of lines that are formed in a deeper part of the photosphere. It can be seen from Table 5 that the highest value of $\Delta v = v_2 - v_1$ is observed for the HeI λ5876 Å lines, and the smallest for the D NaI lines. For the rest lines, including the weak lines of the photosphere, the value of Δv is within 60 km/s^{-1} $\pm$ 20 km/s^{-1}. This indicates that the most active variations

are generated in the higher-temperature regions of the photosphere, where helium lines are formed.

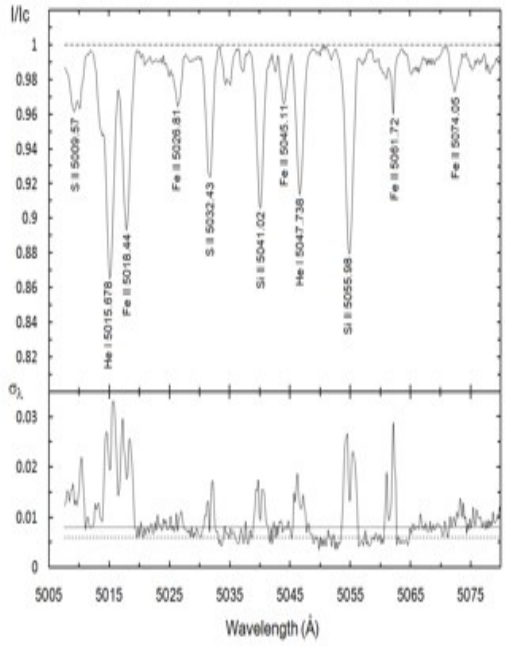

Fig. 4. The average profiles of the spectral region λ5005-5080 Å of the supergiant HD199478, obtained from the 2014 data, containing weak photospheric lines (top panel). Bottom is the TVS structure of this range. In each TVS spectrum, the horizontal bold dashed lines indicate the mean continuum level and the dotted lines belong to the level of the variability threshold equal to p = 1%.

Figure 6 shows the distribution of the mean radial velocities RV , as well as the velocities v1, v2, Vc (Table 6), obtained in 2011 and 2014 for different lines. The horizontal straight dashed line shows the velocity level of the mass center of the star V0 ($-15km/s^{-1}$, [12]). The abscissa shows the numbers according to the list of spectral lines, which are presented in Table 6. Here the lines numbered 1-7 are the strongest lines, which are shown in bold type in Table 6. Numbers 8-19 are weak absorption lines with EW$\leq$0.25 Å. Figure 6 shows that the Vc velocities are always systematically lower than the V0, which indicates a presence of the permanent matter outflow. Also, Vc does not always coincide with RV for different photospheric lines, although, for example, in 2011, the variations in these velocities are synchronous. The observed drift of the velocity Vc for different lines indicates radial wind propagation in different layers of the atmosphere.

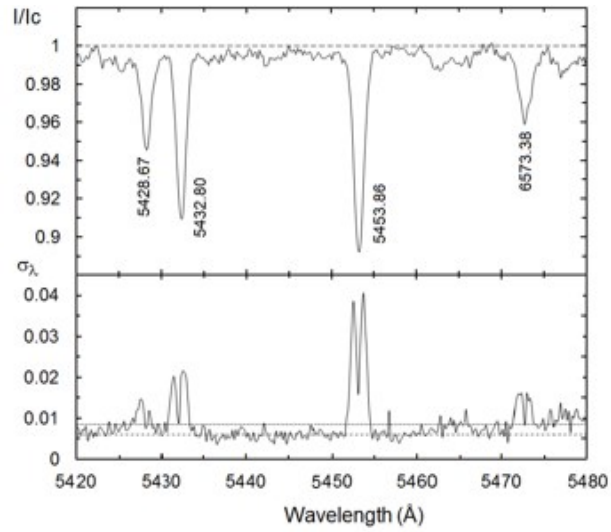

Fig. 5. The same as in Fig.4, for the λ5420-5480 Å spectrum region, obtained in 2014 containing weak photospheric lines (upper panel).

As can be seen from Fig.6, the velocities v_1, and v_2 corresponding to the peaks in the TVS structures for different lines are located symmetrically relative to the Vc velocity. The Vc velocity mainly shows the variation in the mean wind motion in a local area where considered spectral lines are formed.

3.3. Variability of Absorption Lines When Observing HVA

As shown by [6], high velocity deep absorption was detected in the spectrum of HD 199478 in 2011 on the blue wing of the Hα line (HVA). The spectral material obtained allows us to study the variations in photospheric lines in the moment of the observation of this event. Figure 7 shows the time variation diagrams of the radial velocities and equivalent widths of the strongest photospheric lines obtained during 17 nights of observations in 2011. Each line of the panels on the left displays RV variations, on the right - EW variations of individual lines. The top first line on the panels shows the time variations in the parameters of the emission line Hα. This is shown for comparison with the same variations in absorption lines obtained at the same time (Ismailov&Ismayilova, 2019). As can be seen, RVs of the lines CII, HeI, SiII, as well as those of the D NaI line with a delay of maximum (by 12 days), show a smooth variation with an amplitude of 4-8 km/s^{-1}. If we take the velocity of the star mass center -15 km/s^{-1} , then the maximum in the RV variation for most absorption lines will be reached on JD 2455760 $\pm$ 3, at positive values of the radial velocities.

As shown in [6], the HVA event in the star HD 199478 was observed in the time interval JD 2455764-2455776 (about 13 days), the boundaries of which are indicated by two vertical straight lines in Fig. 7. When comparing the data of the Hα line with the data of the strongest absorption lines, we can state that the HVA event appeared right at the moment when RV values of strong absorption lines were maximal and positive, and continued to be observed as long as the RV values were decreasing to the minimum (on JD 2455776). In other words, during the appearance of the blue shift on the wing of the Hα line, a blue shift of many absorption lines is observed, and this state continues until the disappearance of the HVA event. As shown in [6], the HVA event in the star HD 199478 was ob-

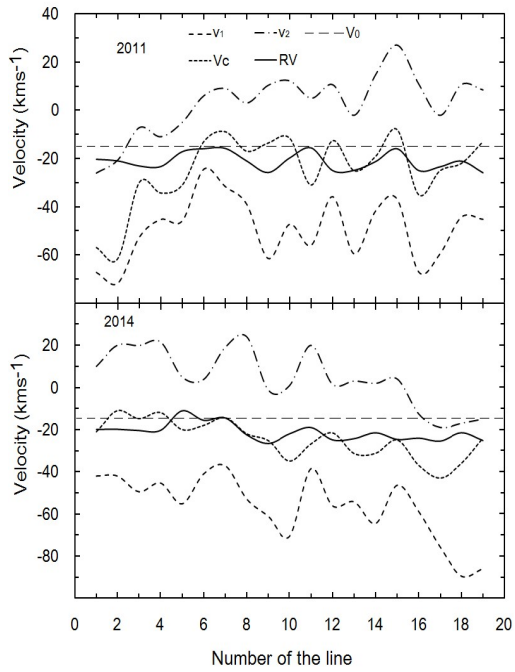

Fig. 6. Distribution of the mean radial velocities RV (solid curve), as well as velocities v_1 (large dotted line), v_2 (dotted line with a dot), Vc (small dotted line) (Table 4A) for different spectral lines according to the data of 2014 (top panel) and 2011 (bottom panel) The abscissas indicate the line number in the list of Table 3.1. The horizontal dashed stright line shows the velocity level of the stellar mass center V0. The top panel refers to the 2011 data, the bottom one, to the 2014 data. The designations of the parameters are the same in all panels.

served in the time interval JD 2455764-2455776 (about 13 days), the boundaries of which are indicated by two vertical straight lines in Fig.4. As can be seen from Fig.7, the RVs of the D NaI lines reach a maximum after the completion of the

HVA event, when the RVs of the remaining lines have already reached their minima. This means that after the completion of the HVA event and the disappearance of the blue shifts in other absorption lines, the D NaI lines exhibit the maximum positive RV value, that is, the accretion process is observed. Figure8, also shows diagrams of time variations in spectral parameters for some weak photospheric lines. It can be seen from the left panels of Fig.8 that the radial velocities for most of the lines exhibit a smooth shift to the blue part of the spectrum, which invariably continues its course during presence of the HVA event. At the end of the HVA event, the RV values of the weak lines reach their minima. The RVs of strong photospheric and Hα lines reach their maxima at the onset of the HVA event (Fig.7), i.e. at the maximal contracted state of the star. During the HVA, both weak and strong absorption lines show blue shifts, i.e. expansion of the star.

The equivalent widths of weak photospheric lines vary in different ways. For example, the EWs of the FeII λ5316 and λ5487 Å lines exhibit an increase, while the SiII λ5041 and λ5056 Å lines show a decrease, and weaker SII lines do not show significant variations during the HVA event at all. This shows that there are relatively stationary regions of the photosphere where weak absorption lines are formed (Fig.8).

Now let us consider the variations in the profiles of absorption lines, according to the data of 2011. The average profiles of individual absorption lines, as well as the results of the obtained TVS spectra σ_λ for 17 nights of observations, are presented in Fig.9. All designations here are the same as in Fig.3. The double peak structure in the TVS spectrum suggests real variations of radial velocities along the spectral lines, in accordance with the velocity range ΔV. The velocities corresponding to the v_1 and v_2 peaks in the TVS spectrum show the most probable values of the RV variations along the spectral line. As can be seen from Fig.6, RV variations on the center at the line are insignificant, and the largest variations occur on the wings of the lines at velocities v_1 and v_2. Judging by the obtained TVS structures, RV variations observed in the velocity range ΔV, suggest that the radial mode gives contribution to the peaks, while the non-radial mode - to the other parts of the profile.

As can be seen from Table 5, the total range ΔV for the CII, SiII, He I lines was about 200 km/s^{-1} in 2011, and for the D NaI lines, about 125 km/s^{-1}. The FWHM of the average profile from the CII, Si II, and HeI lines was 80-90 km/s^{-1}, and much less for the D NaI lines, namely, 50-60 km/s^{-1}. This pattern persists for all other seasons (Table 5).

As can be seen in Fig.9, the average profile of each line of the D Na I doublet consists of one strong and another weak red component. TVS profiles of the spectra of these lines also consist of two components, with the velocities of the first, strong components, corresponding to -19 and -14 km/s^{-1}, which coincide

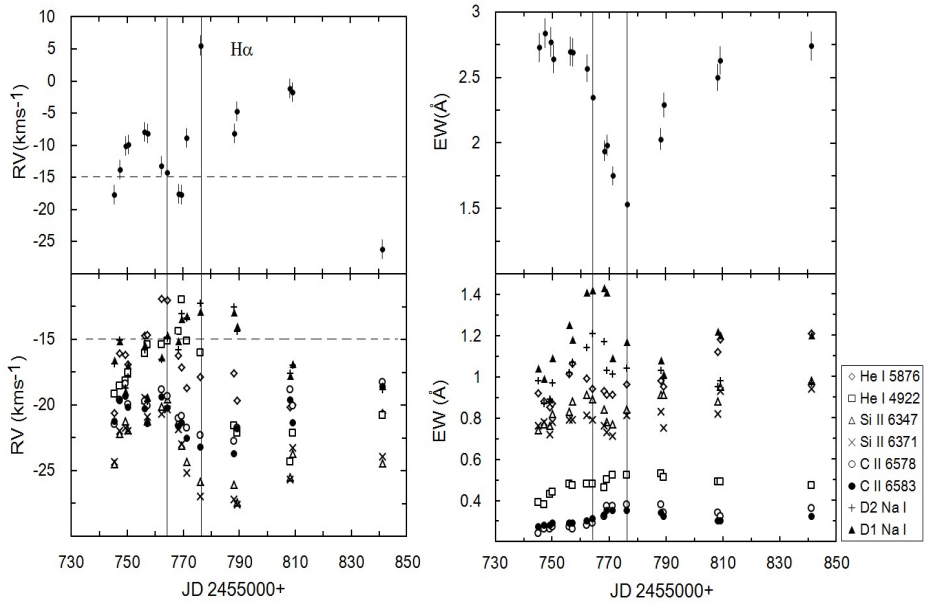

Fig. 7. Time variability in the RV and EW parameters for the emission Hα line (top panels) and for the various strongest photospheric lines (bottom panels), according to 2011 data. Two vertical straight lines indicate the boundaries of the time interval when HVA was observed. The horizontal dashed lines on the left panels indicate the star's mass center velocity.

well with the mass center velocity of the system. And the velocities of the second peaks correspond to 47 and 31 km/s^{-1}, respectively, for the D1 and D2 NaI lines. This indicates that the D NaI doublet lines are formed in the upper part of the stellar wind, and the radial velocities of these lines in 2011 varied insignificantly. The weak red component, rather, is formed in the flow of the upper part of the envelope, showing the fall of matter onto the star at a velocity of about 40 km/s^{-1}.

For weak absorption lines for the seasons 2011, 2013 and 2015 we got similar TVS profiles with 2014 data (Table 5).

4. DISCUSSION AND CONCLUSIONS

Our results for the first time ever, have shown that the scale of temporal variations in photospheric lines is in good coincidence with the quasi-cyclic variability of the emission component of the line Hα. As shown in the work of Markova et al. (2008), the variability of the Hα line cannot be represented as strict periodic. The instability of the periodicity according to the data of different years complicates

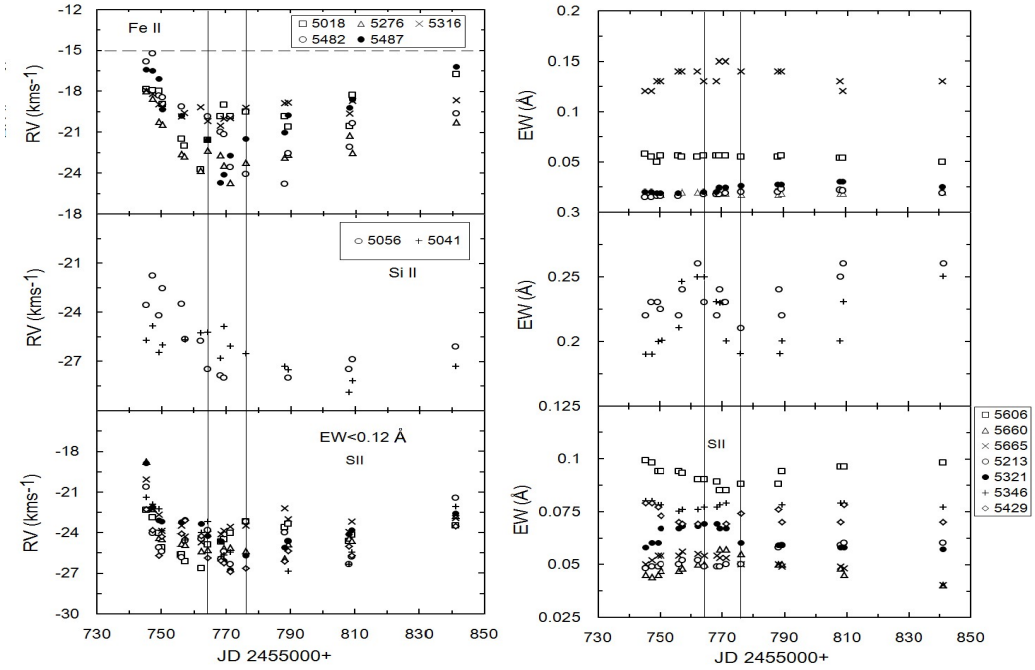

Fig. 8. The same as in Fig.2 for the data of season 2011. Two vertical straight lines indicate the boundaries of the time interval when the HVA was observed. The horizontal dashed line on the left panel indicates the star's mass center velocity.

the obtaining of accurate information about the pulsation modes and astroseismic information, which is required to study the photospheric variability in BA supergiants. Rather, photospheric variability occurs in quasi-cycles, individual fragments of which can be observed. Our data have shown for the first time that the parameters of photospheric lines from minimum to maximum (half cycle), or vice versa, vary over a timescale of about 25 days. In this star we detected the same characteristic time for hydrogen lines [6]. The scale of temporal variations of 40-50 days is typical for the full cycle of variations in hydrogen lines (see Table 2 from [6]. Our data revealed that these time scales are in good agree with absorption lines too.

We have shown that the root mean square deviations σrms of the RV and EW parameters observed over the season for strong photospheric lines is much larger than for weak photospheric lines (Table 2). Therefore, the observed quasicyclic variability is more clearly pronounced in the stronger photospheric lines. For weak lines, which are formed mainly in the lower photosphere, cyclic variations are observed in a weak form or are not observed at all within the measurement uncertainty. This result is typical for all observation seasons. This indicates that

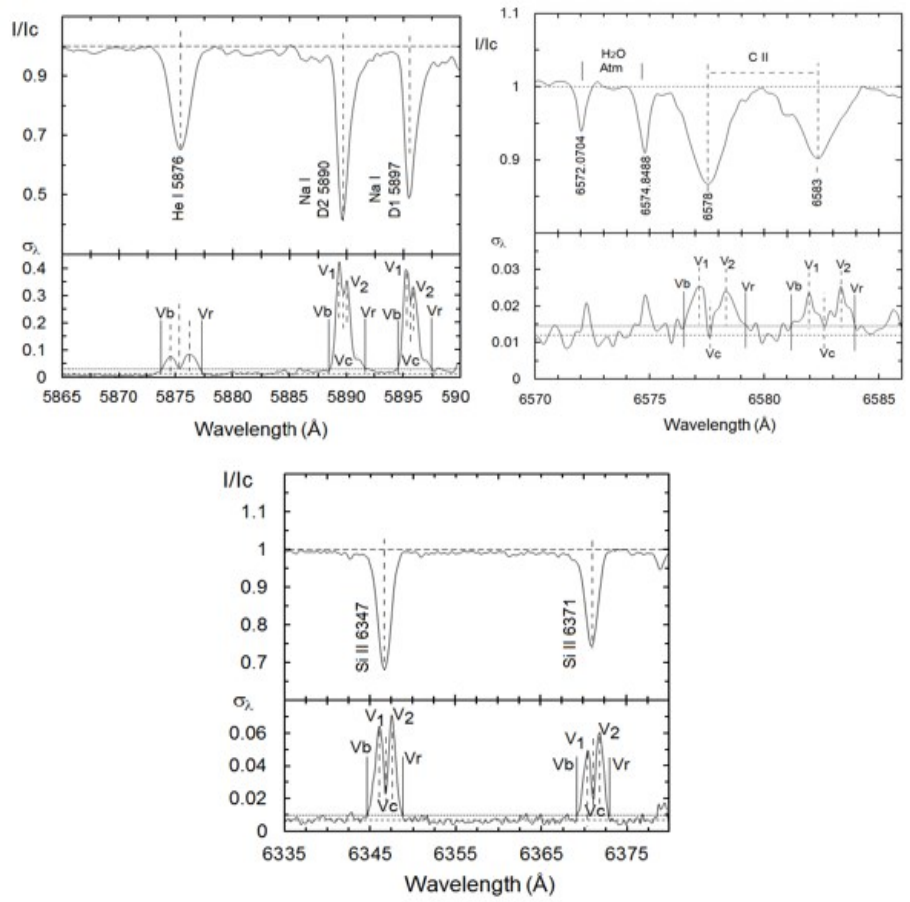

Fig. 9. The same as in Fig. 3 according to 2011 data.

the strongest photospheric lines, which are formed throughout the depth of the photosphere, are more influenced by the stellar wind in the upper photosphere. We have shown that, during the HVA event, the radial velocities of all photospheric lines exhibited an outflow from the star and the equivalent widths of individual photospheric lines were increasing, while in the outer part of the wind, where the Hα emission is formed, EWs were decreasing. This indicates that a possible HVA event started in base of stellar wind and propagated subsequently into the wind. This observational fact is an argument in favor of the assumption on the existence of radial pulsation in such stars.

An analysis of the TVS structures of individual groups of photospheric lines has shown that the radial velocity variability is observed in both strong and most weak photospheric lines. Different absorption lines exhibit different radial velocity variation interval Δv. It has been shown that the highest value of Δv is

observed for the HeI λ5876 Å lines (80-120 km/s^{-1}), and the smallest for the D NaI lines (20-35 km/s^{-1}) (Table 4). For the rest of lines, including weak lines of the photosphere, the value of Δv is in the range of 30-60 km/s^{-1}. This indicates that the most active variations are generated in the higher-temperature regions of the photosphere. As can be seen from Table 3.1, the seasonally averaged value of the velocity interval Δv along all lines is about 60 km/s^{-1}.

The data in Table 5 show that the mean values of the Vc parameter obtained both in 2014, when the star was not affected by the HVA event, and in 2011, when HVA was observed, are close to the observed radial velocities. The observed difference in the velocity Vc for individual lines is obviously related to the local physical conditions (temperature, wind speed, etc.) under which these lines are formed. It can be seen from Table 5 that the average value of the velocity Vc for individual seasons slightly differ from the average radial velocities (see Figure 6). The FWHM values for the absorption lines are larger than the projection of the rotational velocity of the star (Table 5). As was noted in Markova &Puls (2008), this may be partly due to the existence of macroturbulent velocity in the stellar atmosphere. These authors estimated the projection of the rotation velocity vsini $= 41 \pm 4\ k/s^{-1}$, the microturbulent velocity $\sim 8\ km/s^{-1}$, and the macroturbulent velocity about $40 \pm 3\ km/s^{-1}$. By using the expression

$$V(FWHM)[km/s^{(-1)}] = \sqrt{((\nu sini)^2 + \xi^2)} \quad (1)$$

an expected value of the macroturbulent velocity can be found [8]. Here V (FWHM) is the velocity value corresponding to the FWHM, vsini is the projection of the rotation velocity to the line of sight, Ξ is the total velocity component due to the macro- and micro-turbulent velocities. It can be seen from Table 5 that the dominant FWHM value for strong absorption lines is about 2 Å, for weak photospheric lines it is about 1.6 Å, which correspond to velocities of 100 and 96 km/s-1, respectively. Then, from this expression for ξ, a value of $\sim 91 \pm 9\ km/s^{-1}$ can be obtained, which is much larger than the value given in [16]. Therefore, we assume that one of the reasons for the additional expansion of absorption lines is the radial movement of individual clumps in the stellar wind. The existence of a clump-like wind structure in a spherically symmetric atmosphere of supergiants has been noted in different works (see, for example, [1, 8]). An additional argument in favor of this assumption is that in some seasons selected absorption lines showed high stability, while other spectral lines showed certain variability. This suggests that there are zones of local formations, with different physical conditions in the atmosphere of the star. The existence of radial motion of matter also follows from the structure of the Hα emission component, which often shows two peaks with a variable V/R ratio [6, 8]. Such wavelike variations,

accompanied by the cyclic movement of matter, indicate that the structure of the stellar atmosphere is not spherically symmetric and does not have any stationary wind (see, for example, Morel et al. [16,17].

Knowing the assumed value of the quasi-period P_ν in days, the amplitude of variations in the radial velocities of absorption lines A_ν in km/s^{-1}, the radius of the star R_* in solar radius, it is possible to estimate the amplitude of the light variation of the star due to the variation in the radius during pulsation [11]. This does not take into account variations in color-indexes. Using the averaged parameters taken from Table 3 for these parameters, we have used the values of 48 ± 10 days, 5 ± 3 km/s^{-1} and 68 $R_\odot$ [15], respectively. By using the expression

$$\Delta m_{rad} = 5log(1 + 0.02\frac{P_{\nu[d]}A_{\nu[km/s^{-1}]}}{R_*[R_\odot]}) \quad (2)$$

for the amplitude of the brightness variation, we can get $\Delta m_{rad} 0.14^{+0.08}_{-0.05} mag$

As can be seen, this value of the light variation is in good agreement with the amplitude of the light variation of 0.15 mag [20], which was obtained from a large number of photometric observations. Hence it follows that the quasiperiodic pulsation of the star seems to be accompanied by a variation in the radius, the magnitude of which can be measured from the radial velocities of the photospheric lines.

The question of the main reason for the activity in the star's atmosphere remains open. Given the above, to explain the observed spectral variations, we tend to accept the concept of the appearance of inhomogeneity on the surface of the star. For the explanation of the observed results, apparently, the magnetic field can play a key role. Measurements of the longitudinal magnetic field BA type SGs show that the maximum value of the magnetic field strength for β Ori is 130 G, and for the remaining BASGs it is several gauss (see, for example, [23]). However, the inhomogeneity on the surface of the star can be caused by spots, where the local magnetic field is much higher.

So, based on the results of this work, the following conclusions can be drawn:

1. After having studied the spectrum of the supergiant HD 199478, we have established for the first time that variations in the radial velocities of photospheric lines and lines that are indicators of stellar wind (emission in the Hα line) occur synchronously. An inverse correlation has been revealed in the behavior of the equivalent widths of strong photospheric lines and the emission component of the Hα line. Weak absorption lines formed in the lower photosphere do not always indicate to a synchronous motion in the lower and upper photosphere.

2. The time scale of variations in radial velocities and equivalent widths of photospheric lines are in good agreement with the time of variations in the Hα line. The

variation of the parameters of spectral lines occurs in quasiperiodic cycles, which are characterized by maxima and minima. The timescale of variation from one extrema to another is about 25 ± 4 days. The timescale of the full quasi-period is 45 ± 10 days. The amplitude of variations in radial velocities and equivalent widths for strong absorption lines is much larger than for weak absorption lines.
3. It was shown for the first time that during the HVA event, both strong and weak photospheric lines show a blue shift relative to the center of mass of the system. The same shift is observed in the emission component of the Hα line. This suggests that a mass-loss event highly likely started at the base of the stellar wind with subsequent propagation into the wind.
4. The TVS structure of photospheric lines show that the variation in radial velocities most often manifests on the wings of photospheric lines, which is expressed by the appearance of two peaks on the TVS profiles. The distribution of the velocity gradient along the line show the existence of radial and non-radial pulsations. Localization of the velocity gradient on the wings of photospheric lines can be a consequence of rotational modulation due to the inhomogeneous surface of the photosphere.
5. The D NaI lines most likely form in the upper part of the wind, indicating from time to time to signs of the matter accretion to the star's surface.
6. The performed analysis has shown that the reason for the large expansion of photospheric lines may be a clumpy structure of the stellar wind.
7. The photometric variability of the star can be explained by the cyclical variation of the stellar radius, which confirms the existence of radial pulsations in the stellar atmosphere.

5. ACKNOWLEDGEMENTS

This work was supported by the Science Development Foundation under the President of Azerbaijan – Grant № EIF-BGM-4-RFTF- 1/2017-21/07/1.

REFERENCES

1. Chesneau O., Kaufer A., Stahl O. et al., 2014, A&A 566, A125

2. Denizman L., Hack M., 1988, A&AS 75, 79

3. Fullerton A.W., Gies D.R., Bolton C.T., 1996, ApJS 103, 475

4. Galazutdinov G.A. Preprint SAO RAS, 1992, № 92

5. Ismailov N.Z., Bahaddinova G.R., Kalilov O.V., Mikailov Kh.M., 2013, Astrophysical Bulletin, 68, № 2, 196

6. Ismailov N.Z., Ismayilova Sh.K. 2019, MNRAS, 485, 3558

7. Ismailov N. Z., Pogodin M. A., Bashirova U. Z., Bahaddinova G. R. 2020, Astron.Reports, 64, 23I

8. Israelian G., Chentsov E., Musaev F., 1997, MNRAS, 290, 521

9. Kaufer A., Stahl O., Wolf B., et al. 1996a, A&A, 305, 887

10. Kaufer A., Stahl O., Wolf B., et al. 1996b, A&A, 314, 599

11. Kaufer A., Stahl O., Wolf B., et al. 1997, A&A, 320, 273

12. Kharchenko N. V., Scholz R. D., Piskunov A. E. et al. 2007, AN 328, 889

13. Markova N., Valchev T., 2000, A&A, 363, 995

14. Markova N., Prinja R. K., Markov H., et al. 2008, A&A 487, 211

15. Markova N., Puls J., 2008, A&A 478, 823

16. Markova, N., Puls, J., Repolust, T., et al. 2004, A&A, 413, 693

17. Markova, N., Puls, J., Scuderi, S., et al. 2005, A&A, 440, 1133

18. MikailovKh. M., Khalilov V. M., Alekberov I.A., Tsirk. ShAO, 2005,109, 21

19. Morel T., Marchenko S. V., Pati A. K. et al. 2004, MNRAS, 351, 552

20. Percy J., Palaniappan R., Seneviratne R.et al. 2008, PASP, 120, 311

21. Prinja R.K., Fullerton A.W., Crowther P.A., 1996, A&A 311, 264

22. Rosendhal J.D., 1973, ApJ 186, 909

23. Shultz M.,Wade G. A., Grunhut J., et al.MiMeS Collaboration, 2012, ApJ, 750, 2